



# Modeling and Optimization of Process Parameters for Laser Powder Bed Fusion of AISi10Mg Alloy

Mihir Samantaray<sup>1</sup> · Dharendra Nath Thatoi<sup>1</sup> · Seshadev Sahoo<sup>1</sup>

Accepted: 31 July 2019 / Published online: 8 August 2019  
© Springer Science+Business Media, LLC, part of Springer Nature 2019

## Abstract

Direct Metal Laser Sintering (DMLS) is a laser powder bed fusion process, grabs the attention of industries to make metal components directly from the metal powders. However, the quality of the build component depends on the sintering depth as well as sintering mechanism which are directly influenced by process parameters. Proper selection of process parameters to build the component is the key to the success of the DMLS process at commercial level. A common solution to make a quality component is to fuse the powder layers with maximum layered thickness, which can be achieved with appropriate selection of process parameters. In the present research, finite element simulations have been carried out to measure the sintering depth at different process parameters such as laser power, scan speed, porosity percentage, laser spot size, and powder bed thickness. Based on the predicted temperature field and sintering depth, an optimization model was developed by using response surface methodology with an aim to optimize the process parameters that improve the printing quality. The accuracy of the model was confirmed by using analysis of variance. From the optimization model, it is found that maximum sintering depth of 3 mm achieved with a laser power of 162 W, a scan speed of 156 mm/s, the percentage of porosity of 20%, a laser spot size of 0.2 mm, and the powder layer thickness of 1 mm respectively. This optimized model will help to design and control the process parameters for building quality components.

**Keywords** Additive manufacturing · Direct metal laser sintering · Optimization · Surface response method · Thermal modeling

---

✉ Seshadev Sahoo  
seshadevsahoo@soa.ac.in

<sup>1</sup> Department of Mechanical Engineering, Institute of Technical Education and Research, Siksha 'O' Anusandhan (Deemed to be University), Bhubaneswar, Odisha 751030, India

## Introduction

In the era of digital manufacturing, additive manufacturing technologies have been successfully adopted in the manufacturing sector to fabricate functional prototypes in layer-based technique. This technology was broadly applicable to all class of materials such as metals, ceramics, polymers, and composites, whereas, for processing of metals, metal-based additive manufacturing recently emerged as an important commercial manufacturing technology [1]. Direct Metal Laser Sintering (DMLS) is a metal-based laser powder bed additive manufacturing process developed by EOS GmbH (Munich, Germany), which fabricates near-net-shape 3D metallic parts directly from the metal powder. A high power laser source is utilized to fuse aluminum, steel, bronze and titanium-based metallic powders layer by layer. The mechanism behind the consolidation of metallic powders in the DMLS process is liquid-phase sintering [2, 3]. To build a three-dimensional component in the DMLS process, first a digital model is created with the help of CAD programme. Then the digital model file is exported from the CAD programme in STL format and print the component. The build components with complex structure and high density can be achieved through sound metallurgical bonding between scanning tracks and subsequent layers. In comparison with traditional manufacturing processes, the DMLS process has design freedom to make components, economic, and energy efficient [4]. However, the quality of the built part in DMLS process depends on the processing parameters i.e., laser power, scan speed, layer thickness, hatch spacing, hatch pattern, the porosity of powder bed, and laser spot size. In order to obtain a quality component in the DMLS process, it necessitates that the part should be fabricated with optimized process parameters.

Earlier researchers have been investigated the influence of processing condition on sintering mechanism, melt pool formation, temperature history, and on build quality in the additive manufacturing process by both numerically and experimentally. Effect of laser power and scan speed on temperature distribution and powder fusion of different metal powders in metal additive manufacturing processes were studied numerically as well as experimentally [5–8]. The authors found that laser power and scan speed are the most influencing parameter to control the build quality. A transient model was developed by Kundakcioglu et al. [9] to explore how the temperature varied in the powder bed by changing the laser scan path. This model helps for process enhancement and optimizations of process parameters to build quality components. Lee et al. [10] formulated a particle-based discrete element model to study the effects of laser power, laser scan speed, and hatch space on the temperature distributions in the powder bed in the DMLS process. From this study, the authors concluded that laser scan speed and hatch space does not have a significant effect on the temperature rise but laser power increases the temperature in the powder bed significantly. Dong et al. [11] developed a finite element model for laser powder bed fusion of Ti powders using ABAQUS platform. Based on the developed model, the process parameters were correctly to avoid the failure of the process. For direct metal laser sintering of AlSi10Mg powders, Ojha et al. [12] developed a transient model which considers fluid flow, heat transfer, and solidification characteristics in the liquid pool and investigated the densification mechanism of the build part. Panda and Sahoo [13] developed a thermo-mechanical model to investigate the residual stress formation in the AlSi10Mg powder bed with respect to scan speed and laser power. Based on the residual stress, they optimized the process parameters to minimize the residual stress in the built

part. Samantaray et al. [14] formulated a thermodynamic model to investigate the sintering of AlSi10Mg powders and the thermal behavior in the powder bed during the direct metal laser sintering process. From the simulation, the authors also studied the molten pool profile, temperature distribution, and sintering depth, which help to optimize the thickness of the powder layer and thereby reducing the wastage of powder material.

In addition, researchers have been attempted to optimize the processing conditions in different additive manufacturing processes to enhance the part quality. Dong et al. [15] used the Taguchi method to optimize the process parameters in the fused deposition modeling process. To find the optimal process parameters which improve the printing quality, the authors used S/N ratio analysis. A physics-based model for laser powder bed fusion process was developed by Criales et al. [16] to calculate the temperature along the scan path and hatch directions. Further, their model was validated with experimental analysis. Predicted temperature field from the simulation model was utilized to optimize the process parameters using response surface methodology. Effect of process parameters on the relative density of AlSiMg0.75 alloy build parts in selective laser melting process were studied by Bai et al. [17]. The authors used the design of experiment using response surface method to optimize the selective laser melting process parameters for obtaining the maximum relative density. Verma et al. [18] used a bi-criteria-based optimization approach to optimize part orientation, layer thickness identification, and laser scanning directions with an aim to build the parts with a minimum amount of time and minimum surface inaccuracy in the direct metal laser sintering process.

From the above literature review, it was found that laser power, scan speed, hatch distance, laser spot size etc. are the important processing parameters to control the quality of the built part. But, due to the lack of research information related to the effect of process parameters on the quality of the built part, till now no guidelines were established to find the optimal process parameters for the fabrication of parts in DMLS process. Therefore, it necessitates investigating the relationship between process parameters with the quality of built parts and optimizes the processing parameters to fabricate quality parts. The objective of this paper is to optimize the process parameters for manufacturing of components in the DMLS process. The optimization will be carried out using response surface methodology. This model will be considered as a guideline for the manufacturing of components in the DMLS process.

## Modeling of Temperature Distribution in the Direct Metal Laser Sintering Process

The purpose of finite element based modeling is to calculate the sintering depth based on temperature distribution in the AlSi10Mg powder bed in the direct metal laser sintering process. Finite element simulations of heat transfer in DMLS processes is carried out by solving the energy equation, which describes temperature ( $T$ ) as a function of  $x$ ,  $y$ ,  $z$  and time ( $t$ ):

$$\frac{\partial}{\partial x} \left( k \frac{\partial T}{\partial x} \right) + \frac{\partial}{\partial y} \left( k \frac{\partial T}{\partial y} \right) + \frac{\partial}{\partial z} \left( k \frac{\partial T}{\partial z} \right) + \dot{Q}(x, y, z, t) = \rho C_p \frac{\partial T}{\partial t} \quad (1)$$

where  $k$  is the effective thermal conductivity of the powder bed,  $T$  is the temperature of the powder system,  $\dot{Q}(x, y, z, t)$  is the rate of the internal heat generation per unit volume within the powder bed,  $\rho$  is the material density,  $C_p$  is the specific heat capacity and  $t$  is the interaction time between the laser beam and powder material.

When the laser beam strikes on the top surface of the powder bed, heat generation takes place and it can be modeled in the form of heat flux. In this model, the input heat source follows a Gaussian distribution [19]. The mathematical expression of the input heat flux  $q$  can be defined

$$q(r) = \frac{2AP}{\pi r_0^2} e^{-2r^2/r_0^2} \quad (2)$$

where  $A$  is the laser absorptance of the powder system,  $P$  is the laser power,  $r_0$  is the radius of the laser beam and  $r$  is the radial distance between the laser beam and the center of the spot generated on the top surface of the powder bed, which is calculated using the following relation:

$$r^2 = (|x| - |V \cdot t|)^2 + |y|^2 \quad (3)$$

where  $|x|$  and  $|y|$  represent the distance along X-axis and Y-axis in the powder bed respectively, and  $V$  represents the scan speed of the laser beam.

Considering the process of operation, the following initial and boundary condition are considered for the process simulation. At time  $t=0$ , the substrate and the powder bed is at room temperature, i.e.,

$$[T(x, y, z, t)]_{t=0} = T_0 \quad (4)$$

where  $T_0$  is the ambient temperature. There will be heat loss due to convection and radiation which are considered as boundary conditions in the model.

Heat loss due to convection:

$$q_{\text{conv}} = h(T - T_a) \quad (5)$$

where  $h$  is the convective heat transfer coefficient,  $T$  is the temperature of the top surface of powder bed and  $T_a$  is the ambient temperature.

Heat loss due to radiation:

$$q_{\text{rad}} = \varepsilon \sigma (T^4 - T_a^4) \quad (6)$$

where  $\varepsilon$  is the emissivity of the powder bed,  $\sigma$  is the Stefan-Boltzmann constant for radiation.

Heat lost from bottom surface:

The net amount of heat loss from the bottom surface is as follows:

$$\left[ K \left( \frac{\partial T}{\partial Z} \right) \right]_{\text{at}(Z=0)} = 0 \quad (7)$$

where  $K$  is the thermal conductivity in W/mK.

If the temperature of the powder bed undergoes solid-liquid transition, then liquid state sintering may take place. During solid-liquid phase transformation of powder particles, the material can absorb or release a large amount of latent heat which cannot be neglected in the process. For the simulation of latent heat of phase transformation, the enthalpy can be calculated by using the following equation [20]:

$$H = h + \Delta H \quad (8)$$

where  $H$  is the enthalpy,  $h$  is the sensible enthalpy, and  $\Delta H$  is the latent heat. The sensible enthalpy  $h$  is calculated as:

$$h = h_{ref} + \int_{T_{ref}}^T C_p dT \quad (9)$$

In the above equation,  $h_{ref}$  is the reference enthalpy and  $C_p$  is the specific heat at constant pressure.

The governing equations for thermal analysis were discretized and solved by finite element method using ANSYS 17.0. Figure 1 shows the schematic diagram of the DMLS process and the computational domain used for simulation. The simulation domain consists of the substrate having the dimension of 3 mm × 3 mm × 2 mm and powder layer having the dimension of 3 mm × 3 mm × 1 mm. Considering the computational precision and simulation efficiency, tetrahedral mesh structure was obtained for powder bed with fine meshing and hexahedral mesh for substrate was obtained with medium mesh. The three-dimensional simulation model has meshed into 23,149 nodes and 76,121 elements in all. In the current simulation, the powder bed was considered as multicomponent AlSi10Mg alloy powder and the substrate was made up of structural steel. The detailed modeling procedure including initial and boundary conditions was described elsewhere [14, 21].

## Optimization Using Response Surface Methodology

Optimization is a key tool in engineering which helps to make a decision for process design through the deep understanding of the process parameters. To achieve the quantitative relationship between the input and the output variables, the response

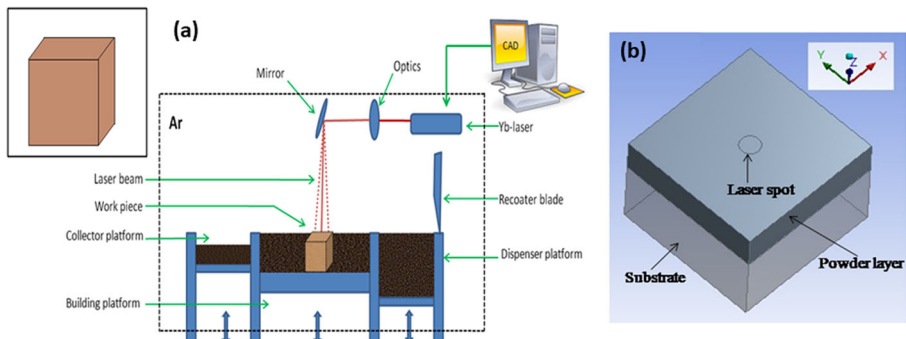


**Fig. 1** a Schematic diagram of the DMLS process (b) Computational domain used for simulation

surface methodology (RSM) is used. Response Surface Methodology is a collection of statistical and mathematical techniques useful for developing, improving, and optimizing processes. By careful design of experiments, the objective is to optimize a response (output variable) which is influenced by several independent variables (input variables). The most extensive applications of RSM are in the particular situations where several input variables potentially influence some performance measure or quality characteristic of the process. The input variables are sometimes called independent variables, and they are subject to the control the process. The field of response surface methodology consists of the experimental strategy for exploring the space of the process or independent variables, empirical statistical modeling to develop an appropriate approximating relationship between the yield and the process variables, and optimization methods for finding the values of the process variables that produce desirable values of the response [22, 23]. The RSM can build the relationship between the input variable  $x$  and the response (output variable)  $y$  with a response function  $f$ .

$$y = f(x_1, x_2, x_3) \quad (10)$$

where  $x_1, x_2, x_3$  are the total number of input variables and  $y$  is the response value. The response surface  $Y$  can be expressed by a second-order polynomial to obtain the equation between input and output parameters. The generalized second order polynomial equation is given as

$$Y = a_0 + \sum a_j x_j + \sum a_{ii} x_{ii}^2 + \sum a_{ij} x_i x_j \quad (11)$$

where  $Y$  is the predicted response,  $x_i$  and  $x_j$  are the coded values of the independent variables, and  $a_0, a_j, a_{ii}$ , and  $a_{ij}$  are the regression coefficient for the intercept, linear and quadratic terms, respectively. The purpose of the experiment is to obtain the maximum  $Y$  value.

The procedures for designing the response surface methodology are following as:

- (i) Identification of the key process parameters,
- (ii) Selection of the upper and lower limit of the process parameters,
- (iii) Selection of output selection response,
- (iv) Developing simulation for design matrix,
- (v) Recording the output response,
- (vi) Developing a mathematical model to relate the process parameters to the output response,
- (vii) Optimizing the model.

## Results and Discussions

### Measurement of Sintering Depth from the Thermal Simulation

In the DMLS process, a high energy heat source is utilized to consolidate the powder particles, which melts and fuse the powders within the fraction of seconds. So, liquid state sintering occurs as the temperatures are high enough to melt the powders and fuse

in. Due to liquid state sintering, shrinkage and densification result from bulk transport mechanisms. In the DMLS process, the temperature distributions in the powder bed and in the substrate are the key issues to the product quality. The temperature distribution along the powder layer height (Z-direction) can provide useful information for measuring the sintering depth. The simulations are carried out by varying the scan speed, laser power, laser spot size, powder layer thickness, and percentage of porosity present in the powder bed. The detailed simulation parameters and thermo-physical properties of AlSi10Mg alloy powders are given in Table 1 and Table 2.

The thermal conductivity and density of a loose powder bed is an important material property for the determination of accuracy of the simulation results. So the thermal conductivity and density of the powders are determined by using the following relation [6, 16, 26]:

$$k_p = k_s(1-\varphi) \quad (12)$$

$$\rho_p = \rho_s(1-\varphi) \quad (13)$$

where  $k_p$  and  $k_s$  are the thermal conductivities of the powder bed and solid material,  $\rho_p$  and  $\rho_s$  are the densities of the powder bed and solid material, and  $\varphi$  is the porosity of the powder bed. Based on the above equations, the thermal conductivity and density of the powder bed is calculated and incorporated in the model. These correlations are used by previous researchers Li & Gu [6], Criales et al. [16], and Hussein et al. [26] and they were taken AlSi10Mg powders for their study.

The temperature distribution on the top surface of the powder layer and the substrate are affected by the heat flux generated due to the high-intensity laser beam. To measure the sintering depth along the thickness of the powder layer, the 3D view of temperature profile on the powder layer as well as the substrate for scanning speed 100 mm/s and laser power of 100 W in DMLS process is shown in Fig. 2a.

The temperature distribution in the melt pool region is shown in different colors. The temperature is higher in the center of the melt pool region than in the other regions. The temperature contours on the top surface of the molten pool are looks similar to a series of ellipses and the ellipses are more intensive in the laser scan direction. At the center of the molten pool, the AlSi10Mg alloy powder is in completely liquid form. For

**Table 1** Process parameters of DMLS process

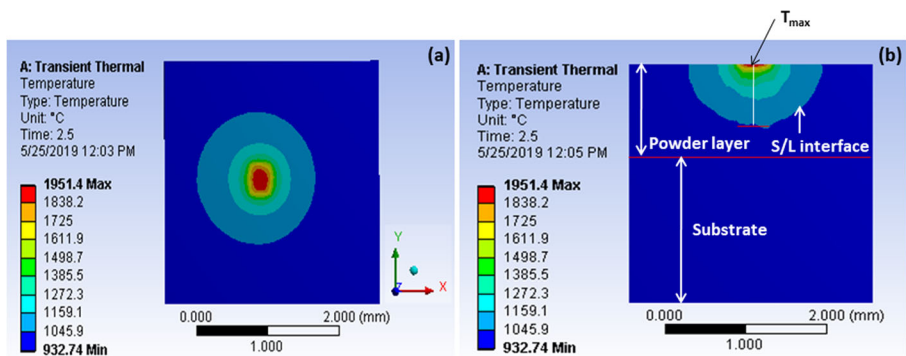
Parameters	Values
Laser Power (W)	70, 100, 130,160,190
Scanning speed (mm/s)	100, 200, 300, 400, 500
Laser spot size (mm)	0.2, 0.3, 0.4, 0.5, 0.6
Thickness of layer (mm)	1, 1.5, 2, 2.5, 3
Percentage of porosity	5, 10, 15, 20, 25
Laser absorptivity	0.09 [6, 20, 24, 25]

**Table 2** Thermo-physical properties of AlSi10Mg alloy [6, 21]

Temperature	20 °C	100 °C	200 °C	300 °C	400 °C
Thermal conductivity( $k$ ), W/mK	147	155	159	159	155
Specific heat capacity ( $c_p$ ), J/kgK	739	755	797	838	922
Heat transfer coefficient ( $h$ ), W/m <sup>2</sup> K	80				
Density ( $\rho$ ), g/m <sup>3</sup>	2.67				
Emissivity ( $\epsilon$ )	0.3				

AlSi10Mg, the liquidus temperature is used to define the melt pool boundary. As liquid phase sintering takes place in this process, the powders are completely melted and fused or sintered beyond the liquidus temperature. So the liquidus boundary is considered as the sintered layer boundary as shown in Fig. 2b. Based on the liquidus boundary along the powder layer thickness direction (Z-direction), the sintering depth for particular powder layer thickness can be obtained. Further, the simulations are carried to know the temperature distribution in the powder layer by varying the scan speed, laser power, laser spot size, powder layer thickness and percentage of porosity present in the powder layer. From the simulation, the thermal profiles are extracted and the sintering depth is measured from the cross-sectional view of the thermal profile by using ImageJ software. Figure 3 shows the measured sintering depth with varying process parameters.

Figure 3a shows the plot of sintering depth in the powder layer with varying laser power. When the laser power is 70 W, the temperature is 731 °C and the sintering depth is 0.06 mm. Similarly, when the laser power is 190 W, the sintering depth is 0.872 mm which is clearly indicated in Fig. 3a. So, it is found that the laser power strongly affects the temperature and sintering depth values in a positive way. Based on the sintering depth, the thickness of the powder layer is optimized as per the requirement for a particular processing condition. So, the wastage of the powders in the DMLS process can be minimized. Figure 3b shows the sintering depth with the scan speed. From the graph, it is observed that, when the laser power is constant i.e. 100 W, by increasing the scan speed, the sintering depth decreases. Further, the quantitative results evidence that the decreasing of sintering depth becomes less prominent as the scan speed is increased

**Fig. 2** a Thermal profile of AlSi10Mg powder layer, b Cross-sectional view of the thermal profile



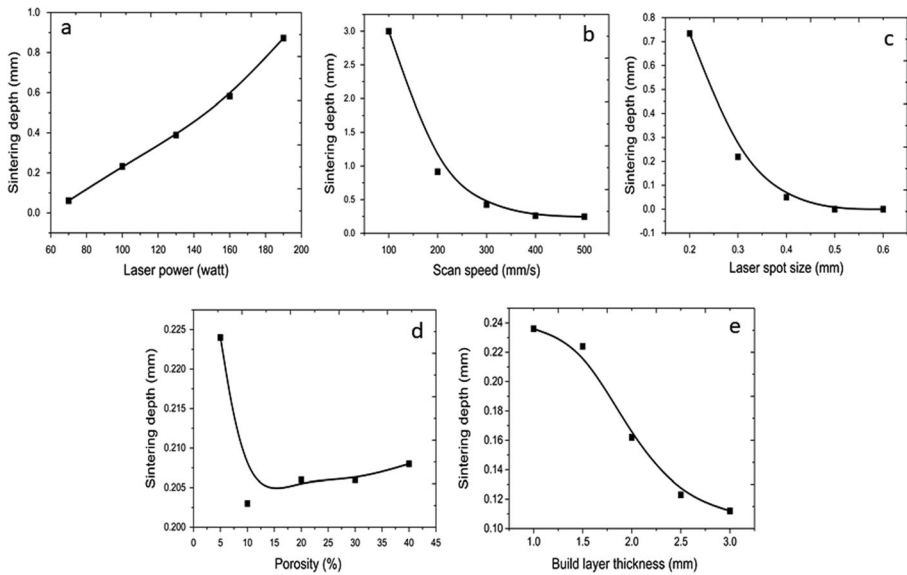


**Fig. 3** Sintering depth with different process parameters (a) varying scan speed, (b) varying laser power, c varying laser spot size, d varying % of porosity, and (e) varying build layer thickness

above 100 mm/s. As the laser energy density is dependent on scanning speed, with an increase in scan speed, the laser energy density decreases and hence the sintering depth is also decreased. This can be clearly seen in Fig. 3b. This is happened because of the decrease in interaction time between the powder particle and laser beam. Similarly, with an increase in laser spot size, the percentage of porosity present in the powder bed and the powder layer thickness by keeping all other parameters constant, the sintering depth also decreases which is clearly observed in Fig. 3c, d and e. This is happened because of the decrease in laser beam intensity. So less amount of heat supplied to the powder bed, as a result, the sintering depth decreases.

### Optimization of Process Parameters

For the process parameters optimization, five process parameters such as laser power, scan speed, laser spot size, build layer thickness and percentage of porosity present in the powder bed was considered. Thermal simulations were carried out by taking permutations of these process parameters which focused to build the matrix on the basis of five levels of laser sintering parameters are mentioned in Table 3. Central composite design (CCD) is a kind of response surface methodology, which has high flexibility and effectiveness [21]. So it is adopted to design the experiment with minimum three factors (A, B, and C) and five levels ( $-\alpha$ ,  $-1$ ,  $0$ ,  $1$ , and  $+\alpha$ ) by Design-Expert program. 32 number of simulations were carried out and from the simulation results, sintering depth was measured which are given in Table 4.

The Design-Expert programme was used to model the simulation results and the best fitting model was selected based on the central composite method with the quadratic polynomial. The sintering depth along the thickness of the AlSi10Mg powder layer is considered as the response value by using multiple linear regression models. The

response value can be obtained as

$$\begin{aligned}
 Y = & 1.70 + 0.56*A - 0.53*B + 0.053*C - 0.43*D - 0.16*E \\
 & + 0.13*A*B - 0.066*A*C + 0.049*A*D \\
 & + 0.058*A*E - 0.061*B*C - 0.16*B*D - 0.047*B*E - 0.11*C*D - 0.096*C*E \\
 & + 0.12*D*E + 0.43*A^2 - 0.065*B^2 - 0.16*C^2 + 0.16*D^2 - 0.16*E^2
 \end{aligned}
 \tag{14}$$

where  $Y$  is the sintering depth;  $A$  is laser power;  $B$  is scan speed;  $C$  is porosity percentage,  $D$  is the laser spot size, and  $E$  is the build layer thickness. Equation (14) was analyzed by using analysis of variance (ANOVA) and a test of significance. In this study  $P < 0.05$  is considered as the significant item. The simulated results show the effect of laser power, scanning speed, laser spot size, build layer thickness, and percentage of porosity on sintering depth as well as the interaction between themselves.

Table 5 represents the ANOVA results of each of process parameter in DMLS process. In Table 5,  $df$  represents the degrees of freedom i.e.,  $df = N - 1$ , where  $N$  is number of sample observations;  $F$  represents the ratio of mean square treatment (MSTR) to the mean square error (MSE) i.e.,  $F = MSTR / MSE$ ,

where  $MSTR = SSTR / (t - 1)$  and  $MSE = SSE / (N - t)$ ,

$SSTR$  is the treatment sum of squares,  $SSE$  is the error sum of squares, and  $t$  is the total number of sample treatments.

$P$  is the probability value, which tells the probability of obtaining an  $F$  value as extreme or more extreme as the one observed under the assumption that the null hypothesis is true.

From Table 5, it is observed that laser power, scan speed, laser spot size, and build layer thickness have a major effect on the sintering depth. Also, it is cleared that  $A$ ,  $B$ ,  $D$ ,  $E$ ,  $AB$ ,  $AC$ ,  $AE$ ,  $BC$ ,  $BD$ ,  $CD$ ,  $CE$ ,  $DE$ ,  $A^2$ ,  $C^2$ ,  $D^2$ , and  $E^2$  are significant model terms and terms like  $AD$ ,  $BE$  and  $B^2$  have no significance as  $p$  value is greater than 0.05. So for making the model more significant the coefficients of  $AD$ ,  $BE$  and  $B^2$  are not considered. The Model  $F$ -value of 81.38 implies the model is significant. There is

**Table 3** Parameters of matrix building

Process parameter	units	Levels				
		-2	-1	0	+1	+2
Laser power	Watt	70	100	130	160	190
Scan speed	mm/s	100	200	300	400	500
Porosity	%	5	10	15	20	25
Laser spot size	mm	0.2	0.3	0.4	0.5	0.6
Build layer thickness	mm	1	1.5	2	2.5	3

**Table 4** Parameters and sintering depth matrix

Run	Laser power (watt)	Scan speed (mm/s)	Porosity %	Laser spot size (mm)	Build layer thickness (mm)	Sintering depth(mm)
1	130	300	15	0.6	2	1.45
2	190	100	5	0.6	3	2.85
3	130	300	15	0.4	2	1.61
4	130	500	15	0.4	2	1.21
5	70	100	5	0.6	1	1.54
6	130	300	15	0.4	1	1.82
7	190	100	25	0.6	1	2.60
8	130	300	15	0.4	2	1.61
9	70	500	5	0.6	3	0.01
10	70	300	15	0.4	2	1.65
11	70	500	25	0.6	1	0.20
12	130	300	15	0.4	2	1.61
13	130	300	25	0.4	2	1.61
14	130	300	15	0.4	2	1.61
15	70	100	25	0.2	1	3.00
16	70	500	25	0.2	3	1.02
17	130	300	15	0.4	2	1.61
18	130	300	15	0.2	2	2.40
19	190	100	25	0.2	3	3.00
20	190	300	15	0.4	2	2.75
21	70	100	25	0.6	3	1.60
22	130	300	5	0.4	2	1.61
23	70	500	5	0.2	1	1.42
24	130	300	15	0.4	3	1.40
25	190	500	25	0.6	3	1.20
26	130	100	15	0.4	2	2.20
27	130	300	15	0.4	2	1.61
28	190	500	25	0.2	1	3.00
29	190	100	5	0.2	1	3.00
30	70	100	5	0.2	3	1.85
31	190	500	5	0.2	3	2.40
32	190	500	5	0.6	1	1.60

only a 0.01% chance that a “Model F-Value” this large could occur due to noise. Values of “Prob > F” less than 0.0500 indicate model terms are significant. Values greater than 0.1000 indicate the model terms are not significant. The “R-Squared” of 0.9933 is in better agreement. And also the “Pred R-Squared” of 0.8378 is in reasonable agreement with the “Adj R-Squared” of 0.9811 which indicates good predictability. Based on the

**Table 5** Analysis of variance for the response surface model

Source	Sum of Squares	df	Mean Square	F Value	<i>p</i> value	Prob > F
Model	17.1286062	20	0.85643031	81.38263573	< 0.0001	Significant
A-Laser Power	5.677326722	1	5.677326722	539.4902623	< 0.0001	
B-Scan Speed	5.0976245	1	5.0976245	484.4038247	< 0.0001	
C-Porosity	0.050033389	1	0.050033389	4.754442965	0.0518	
D-Laser spot size.	3.590306722	1	3.590306722	341.1703448	< 0.0001	
E-Build layer thickness	0.450933389	1	0.450933389	42.85012721	< 0.0001	
AB	0.272745063	1	0.272745063	25.9177096	0.0003	
AC	0.068775062	1	0.068775062	6.535378061	0.0267	
AD	0.038907562	1	0.038907562	3.697206824	0.0808	
AE	0.053940062	1	0.053940062	5.125676201	0.0448	
BC	0.058927562	1	0.058927562	5.599615401	0.0374	
BD	0.412485063	1	0.412485063	39.19655948	< 0.0001	
BE	0.035062562	1	0.035062562	3.331834147	0.0952	
CD	0.191625063	1	0.191625063	18.20924887	0.0013	
CE	0.146497563	1	0.146497563	13.92098998	0.0033	
DE	0.218790063	1	0.218790063	20.79061396	0.0008	
A <sup>2</sup>	0.455155013	1	0.455155013	43.25128878	< 0.0001	
B <sup>2</sup>	0.010373249	1	0.010373249	0.985722139	0.3421	
C <sup>2</sup>	0.062938053	1	0.062938053	5.980713839	0.0325	
D <sup>2</sup>	0.059176582	1	0.059176582	5.623278579	0.0371	
E <sup>2</sup>	0.062938053	1	0.062938053	5.980713839	0.0325	
Residual	0.115758519	11	0.010523502			
Lack of Fit	0.115758519	6	0.019293087			
Pure Error	0	5	0			
Cor Total	17.24436472	31				

ANOVA for response surface model, a new multiple linear regression equation was obtained as shown in Eq. (15).

$$\begin{aligned}
 Y = & 1.70 + 0.56*A - 0.53*B - 0.45*D - 0.16*E + 0.13*A*B - 0.066*A*C \\
 & + 0.058*A*E - 0.061*B*C - 0.16*B*D - 0.11*C*D - 0.096*C*E \\
 & + 0.12*D*E + 0.43*A^2 - 0.16*C^2 + 0.16*D^2 - 0.16*E^2
 \end{aligned} \quad (15)$$

Fig. 4a shows that normal probability and studentized residual values are very close to the diagonal distribution, which indicates a good fit. Figure 4b gives a comparison between actual and predicted sintering depth values. The actual and predicted values are evenly distributed on both sides of the diagonal and it satisfies that the multiple linear regression equation which gives the actual sintering depth.

### Response Surface Contour Plot of Sintering Depth at Different Process Parameters

Figure 5a shows the response surface contour plot for the prediction of sintering depth with respect to laser power and scan speed. From the plot, it is observed that, with an increase in laser power (70 W to 190 W), the sintering depth increases by keeping all other parameters constant. With an increase in laser power, more amount of heat is supplied to the powder bed at a particular instant of time. So that it will increase the sintering depth, as the laser power is directly proportional to heat flux. Similarly, the reverse phenomena are observed with varying scan speed. With an increase in scan speed, the interaction time between the powder bed and the laser beam decreases results in less amount of heat supplied at that particular time. So the sintering depth decreases. The variation of sintering depth with respect to laser power and the percentage of porosity present in the powder bed is shown in Fig. 5b. It is found that, as laser power increases from 70 W to 190 W, it leads to increase the sintering depth from 1.27 mm to 2.57 mm approximately by keeping constant porosity of the powder bed i.e. 5%. When the porosity percentage decreases from 25% to 5% with constant laser power, the sintering depth varies from 2.52 mm to 2.55 mm. It is clearly seen that change is

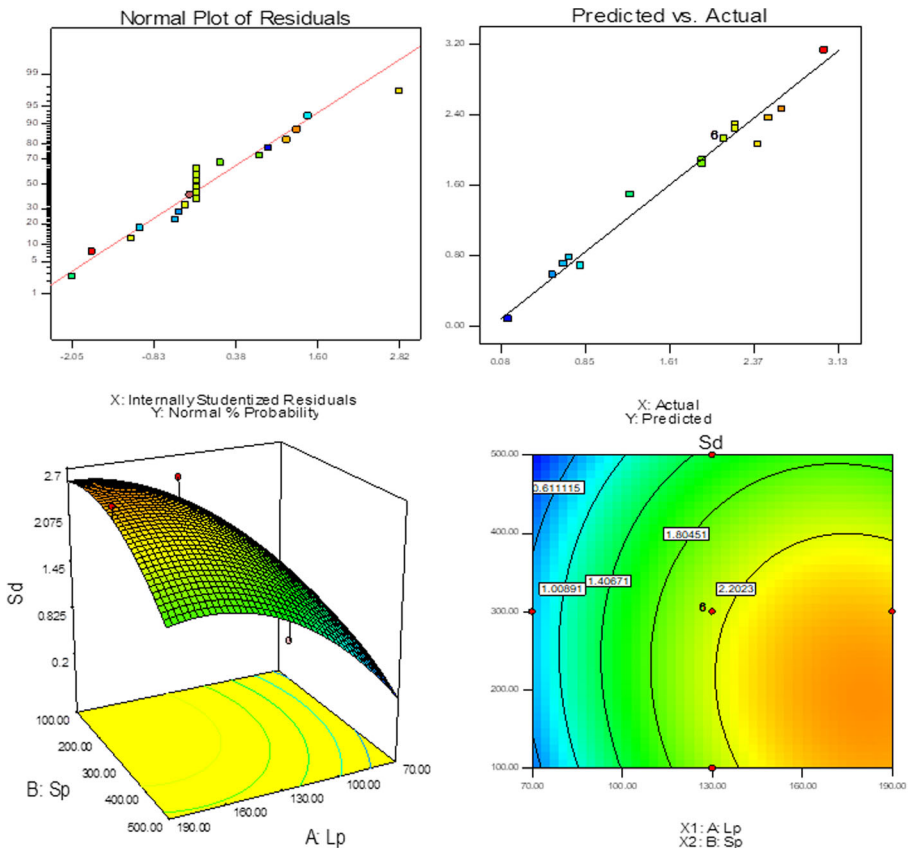


Fig. 4 a Probability distribution of residuals; b Comparison of predicted and actual values of porosity percentage

porosity does not significantly affect the sintering depth. There is a slight change in sintering depth because of the presence of porosity which decreases the conductivity and density of the powder bed. Figure 5c shows that the sintering depth decreases from 3.24 mm to 2.45 mm as laser spot size increases from 0.2 mm to 0.6 mm at a constant laser power 190 watt. The temperature of the top surface of the powder bed depends on the contact area of the laser spot size with powder bed. As the laser beam striking area increases, the energy concentration decreases, and so the surface temperature of the powder bed decreases. Hence sintering depth decreases and also it is found that the powder bed temperature inversely proportional to the laser spot size vice versa. By keeping the laser power constant, the sintering depth of the powder layer decreases from 2.63 mm to 2.43 mm with an increase in powder layer thickness from 1 mm to 3 mm as shown in Fig. 5d. From the contour plot, it is observed that as powder layer thickness increases more amount of heat loss takes place through the powder bed due to the different heat transfer mode such as conduction and convection. So energy intensity on the top surface of the powder bed decreases and causes a decrease in temperature field on the top surface, which results in a decrease in sintering depth.

### Optimization Analysis

During the optimization of process parameters, an objective function was set to maximize the sintering depth. By considering the set of different process parameters such as laser power, scan speed, the percentage of porosity, laser spot size, and build

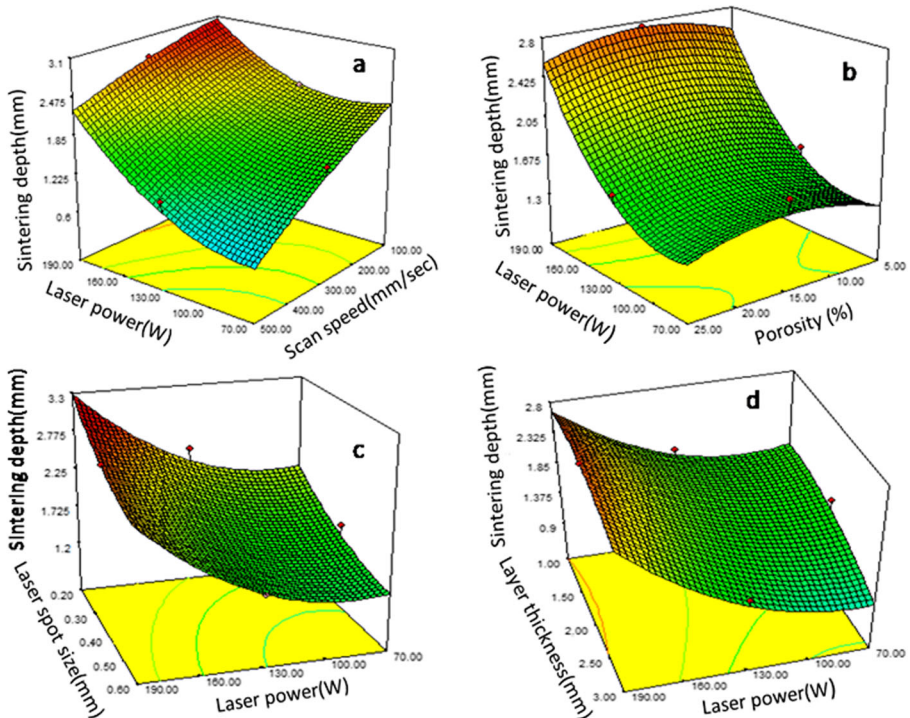


Fig. 5 Response surface contour plot for predicting sintering depth

**Table 6** Numerical optimization results

Number	Laser Power (W)	Scan Speed (mm/s)	Porosity %	Laser spot size (mm)	Build layer thickness (mm)	Sintering Depth (mm)	Desirability
1	161.77	155.78	20.07	0.204	1.03	3.009819456	1 Selected
2	187.04	221.21	24.84	0.29	2.29	3.032918407	1
3	188.88	330	11.37	0.221	2.22	3.010603101	1
4	189.92	315.92	17.24	0.241	2.04	3.080376491	1
5	177.58	106.18	14.62	0.228	2.33	3.025438331	1
6	188.74	112.27	11.23	0.333	1.83	3.038415355	1
7	188.53	101.05	12.65	0.335	2.36	3.016964441	1
8	189.09	109.39	9.16	0.315	1.83	3.024538614	1
9	188.72	330.99	19.16	0.201	2.43	3.036012985	1
10	189.38	385.49	16.97	0.212	2.15	3.034196746	1
11	171.41	101.08	18.08	0.253	1.04	3.003443982	1
12	189.61	277.08	9.87	0.257	1.2	3.002038903	1
13	187.5	169.43	12.8	0.267	2.48	3.008981743	1
14	188.79	328.35	20.92	0.227	2.16	3.028605304	1
15	188.34	244.11	16.44	0.224	2.38	3.105799066	1
16	189.95	133.42	12.42	0.363	1.97	3.012357538	1
17	189.98	100.71	10.31	0.353	2.27	3.001012096	1
18	184.59	308.21	13.31	0.239	1.1	3.000122324	1
19	189.09	185.9	16.34	0.309	1.71	3.085581149	1
20	190	100.01	13.35	0.351	1	2.986716973	0.99555603
21	148.05	100.01	25	0.2	1	2.953397782	0.98440876
22	190	100	9.43	0.49	1.94	2.901760747	0.96713307
23	70	100	17.84	0.226	1	2.779527446	0.92623869
24	70.01	100.11	15.35	0.2	1.92	2.689170344	0.89600881
25	190	266.76	13.56	0.394	1	2.687414771	0.89542147
26	190	270.53	25	0.409	1.78	2.59838343	0.86563514
27	70	111.17	11.12	0.2	2.56	2.310249111	0.76923691
28	70	100	18.54	0.6	2.3	1.952383899	0.6495095
29	70	100	11.34	0.475	2.97	1.754344555	0.58325345
30	70	325.62	5	0.292	2.55	1.326871957	0.44023819

layer thickness the regression model was developed. According to the regression equation model, the optimal process parameters to get maximum sintering depth for AlSi10Mg powder sintering in the DMLS process were obtained by the Design-Expert software: the laser power was 161.77 W, scanning speed was 155.78 mm/s, the percentage of porosity was 20.07%, laser spot size was 0.2 mm, and the build layer thickness was 1.03 mm respectively. Table 6 shows predicted sintering depth with different processing condition. Considering the actual processing precision and ability of the equipment, the optimized parameters of the sintering of AlSi10Mg alloy powders

are as follows: the laser power is 162 W, the scanning speed is 156 mm/s, the percentage of porosity was 20%, laser spot size was 0.2 mm, and the build layer thickness was 1 mm respectively.

## Conclusion

In the present research work, a transient thermal model for direct metal laser sintering of AlSi10Mg alloy was developed using ANSYS 17.0 platform. From the thermal profile, the sintering depth was measured at different process parameters. Statistical design of experiment (DOE) using response surface method was used to get the optimized process parameters in DMLS process and ANOVA analysis was also carried out to determine the significance of each process parameter on sintering depth. The following conclusions are as follows:

- 1) From the simulation results, it is quite evident that the process parameters have a great influence on the quality and property of the sintered part. With increasing laser power, the temperature in the powder bed increases and the sintering depth increases from 0.06 mm to 0.872 mm. A reverse phenomenon observed with increase in scan speed.
- 2) From the thermal model, it is found that there was a variation in sintering depth with respect to different process parameters, which directly influence the properties of the build part.
- 3) Central composite design (CCD) of experiment has been carried out to investigate the effect of DMLS process parameters on the sintering depth of AlSi10Mg alloy and a multiple linear regression model with the sintering depth as the response value is obtained, which performs good fit performance with predicted value of 83.78%, similar to actual value of 98.11%.
- 4) Considering the actual processing precision and ability of the equipment, the optimized parameters of the sintering of AlSi10Mg alloy powders are as follows: the laser power is 162 W, the scanning speed is 156 mm/s, the percentage of porosity was 20%, laser spot size was 0.2 mm, and the build layer thickness was 1 mm respectively.
- 5) From the current research, it can be concluded that optimization of process parameters is necessary for obtaining a good quality product having a smooth surface finish, stability, and greater dimensional accuracy.
- 6) This optimized model will act as a guideline for design and manufacturing of components using different alloy system in the DMLS process and minimizes the wastage of powders used.

## Compliance with Ethical Standards

**Conflict of Interest** On behalf of all authors, the corresponding author states that there is no conflict of interest.

**Replication of Results** No results are presented.



## References

1. Frazier, W.E.: Metal additive manufacturing: a review. *J. Mater. Eng. Perform.* **23**(6), 1917–1928 (2014)
2. Gu, D.D., Meiners, W., Wissenbach, K., Poprawe, R.: Laser additive manufacturing of metallic components: materials, processes, and mechanisms. *Int. Mater. Rev.* **57**(3), 133–164 (2012)
3. Nandy, J., Sarangi, H., Sahoo, S.: Microstructure evolution of Al-Si-10Mg in direct metal laser sintering using phase field modeling. *Adv. Manuf.* **6**(1), 107–117 (2018)
4. Grünberger, T., Domröse, R.: Direct metal laser sintering. *Laser Technol. J.* **12**(1), 45–48 (2015)
5. Shi, Q., Gu, D., Xia, M., Cao, S., Rong, T.: Effects of laser processing parameters on thermal behavior and melting/solidification mechanism during selective laser melting of TiC/Inconel 718 composites. *Opt. Laser Technol.* **84**, 9–22 (2016)
6. Li, Y., Gu, D.: Parametric analysis of thermal behavior during selective laser melting additive manufacturing of aluminum alloy powder. *Mater. Des.* **63**, 856–867 (2014)
7. Zhao, X., Iyer, A., Promopattum, P., Yao, S.C.: Numerical modeling of the thermal behavior and residual stress in the direct metal laser sintering process of titanium alloy products. *Addit. Manuf.* **14**, 126–136 (2017)
8. Sahoo, S., Chou, K.: Phase field modeling of microstructure evolution of Ti-6Al-4V in electron beam additive manufacturing process. *Addit. Manuf.* **9**, 14–24 (2016)
9. Kundakcioglu, E., Lazoglu, I., Rawal, S.: Transient thermal modeling of laser-based additive manufacturing for 3D freeform structures. *Int. J. Adv. Manuf. Technol.* **85**(1–4), 493–501 (2016)
10. Lee, W.H., Zhang, Y., Zhang, J.: Discrete element modeling of powder flow and laser heating in direct metal laser sintering process. *Powder Technol.* **315**, 300–308 (2017)
11. Dong, L., Correia, J.P.M., Barth, N., Ahzi, S.: Finite element simulations of temperature distribution and densification of a titanium powder during metal laser sintering. *Addit. Manuf.* **13**, 37–48 (2017)
12. Ojha, A., Samantaray, M., Thatoi, D.N., Sahoo, S.: Continuum simulation of heat transfer and solidification behavior of AlSi10Mg in direct metal laser sintering process. *IOP Conf. Ser. Mater. Sci. Eng.* **338**, 1–6 (2018)
13. Panda, B.K., Sahoo, S.: Numerical simulation of residual stress in laser based additive manufacturing process. *IOP Conf. Ser. Mater. Sci. Eng.* **338**, 1–6 (2018)
14. Samantaray, M., Sahoo, S., Thatoi, D.N.: Computational modeling of heat transfer and sintering behavior during direct metal laser sintering of AlSi10Mg alloy powder. *C.R. Mécanique.* **346**(11), 1043–1054 (2018)
15. Dong, G., Wijaya, G., Tang, Y., Zhao, Y.F.: Optimizing process parameters of fused deposition modeling by Taguchi method for the fabrication of lattice structures. *Addit. Manuf.* **19**, 62–72 (2018)
16. Criales, L.E., Arisoy, Y.M., Lane, B., Moylan, S., Donmez, A., Özel, T.: Predictive modeling and optimization of multi-track processing for laser powder bed fusion of nickel alloy 625. *Addit. Manuf.* **13**, 14–36 (2017)
17. Bai, Y., Yang, Y., Xiao, Z., Zhang, M., Wang, D.: Process optimization and mechanical property evolution of AlSiMg0.75 by selective laser melting. *Mater. Des.* **140**, 257–266 (2018)
18. Verma, A., Tyagi, S., Yang, K.: Modeling and optimization of direct metal laser sintering process. *Int. J. Adv. Manuf. Technol.* **77**(5–8), 847–860 (2015)
19. Roberts, I.A., Wang, C.J.: A three-dimensional finite element analysis of the temperature field during laser melting of metal powders in additive layer manufacturing. *Int. J. Mach. Tools Manuf.* **49**(12–13), 916–923 (2009)
20. Yuan, P., Gu, D.: Molten pool behaviour and its physical mechanism during selective laser melting of TiC/AlSi10Mg nanocomposites: simulation and experiments. *J. Phys. D: Appl. Phys.* **48**, 1–16 (2015)
21. Panda, B.K., Sahoo, S.: Thermo-mechanical modeling and validation of stress field during laser powder bed fusion of AlSi10Mg built part. *Res. Phys.* **12**, 1372–1381 (2019)
22. Redhe, M., Forsberg, J., Jansson, T., Marklund, P.O., Nilsson, L.: Using the response surface methodology and the D-optimality criterion in crashworthiness related problems. *Struct. Multidiscip. Optim.* **24**(3), 185–194 (2002)
23. Gunst, R.F.: Response surface methodology: process and product optimization using designed experiments. *Technometrics.* **38**(3), 284–286 (1996)
24. Wu, J., Wang, L., An, X.: Numerical analysis of residual stress evolution of AlSi10Mg manufactured by selective laser melting. *Optik.* **137**, 65–78 (2017)

25. Aboulkhair, N.T., Everitt, N.M., Ashcroft, I., Tuck, C.: Reducing porosity in AlSi10Mg parts processed by selective laser melting. *Addit. Manuf.* **1–4**, 77–86 (2014)
26. Hussein, A., Hao, L., Yan, C., Everson, R.: Finite element simulation of the temperature and stress fields in single layers built without-support in selective laser melting. *Mater. Des.* **52**, 638–647 (2013)

**Publisher's Note** Springer Nature remains neutral with regard to jurisdictional claims in published maps and institutional affiliations.